# Weierstraß-Institut
## für Angewandte Analysis und Stochastik
### Leibniz-Institut im Forschungsverbund Berlin e. V.

Preprint ISSN 2198-5855


# Simulations and analysis of beam quality improvement in spatially modulated broad area edge-emitting devices


Mindaugas Radziunas[1], Ramon Herrero[2], Muriel Botey[2], Kestutis Staliunas[2,3]



submitted: April 29, 2014



[1] Weierstrass Institute
Mohrenstr. 39
10117 Berlin, Germany
E-Mail: Mindaugas.Radziunas@wias-berlin.de

[2] Departament de Física i Enginyeria Nuclear
Universitat Politècnica de Catalunya
Rambla Sant Nebridi 22
08222 Terrassa, Spain
E-Mail: ramon.herrero@upc.edu
muriel.botey@upc.edu

[3] Institució Catalana de Recerca i Estudis Avançats (ICREA)
Pg. Lluís Companys 23
08010 Barcelona, Spain
E-Mail: kestutis.staliunas@icrea.cat



No. 1946
Berlin 2014

2010 *Mathematics Subject Classification.* 35Q60 35B27 37M05 78A60 78A45.

2008 *Physics and Astronomy Classification Scheme.* 42.60.By 42.60.Da 42.60.Fc 42.60.Jf.

*Key words and phrases.* semiconductor amplifier, edge emitting lasers, semiconductors, periodic structure, anisotropy, beam shaping, spatial filtering, beam quality.

The work of M.R. was supported by DFG Research Center MATHEON "Mathematics for key technologies: Modelling, simulation, and optimization of real-world processes".

Edited by
Weierstraß-Institut für Angewandte Analysis und Stochastik (WIAS)
Leibniz-Institut im Forschungsverbund Berlin e. V.
Mohrenstraße 39
10117 Berlin
Germany

Fax: +49 30 20372-303
E-Mail: preprint@wias-berlin.de
World Wide Web: http://www.wias-berlin.de/

**Abstract**

We simulate and analyze how beam quality improves while being amplified in edge emitting broad area semiconductor amplifiers with a periodic structuring of the electrical contacts, in both longitudinal and lateral directions. A spatio-temporal traveling wave model is used for simulations of the dynamics and nonlinear interactions of the optical fields, induced polarizations and carrier density. In the case of small beam amplification, the optical field can be expanded into few Bloch modes, so that the system is described by a set of ODEs for the evolution of the mode amplitudes. The analysis of such model provides a deep understanding of the impact of the different parameters on amplification and on spatial (angular) filtering of the beam. It is shown that under realistic parameters the two-dimensional modulation of the current can lead not only to a significant reduction of the emission divergence, but also to an additional amplification of the emitted field.

# 1 INTRODUCTION

Edge emitting broad area semiconductor (BAS) lasers and amplifiers are robust, compact and highly efficient devices for generation of high power beams. However, the spatial and temporal quality of the emitted beams is usually rather low [1, 2]. Several approaches for an improvement of the spatial quality of the radiated optical beam have been proposed and implemented, each, however, with its disadvantages. For example, different schemes of optical injection [3, 4] and optical feedback [5, 6, 7], or integrated narrow master oscillator – tapered power amplifier configurations [8, 9] improve the beam quality, however, in return, the device becomes less compact or rather sensitive to the back reflections. Besides, it has been recently suggested that 2-dimensional modulations of the gain in structured artificial materials enable managing the diffraction of optical beams [10, 11].

In this paper, a theoretical scheme allowing an efficient shaping of the radiated beam is presented. This method implies the compression of the central far-field (FF) lobe down to $\leq 0.5^\circ$ and is based on the (longitudinal and lateral) periodic structuring of the electrical contact [12, 13] (see Fig. 1). It is demonstrated how a proper choice of the spatial periods along with the sufficient modulation amplitude of the gain and the refractive index causes amplification and spatial (angular) filtering of the beam.

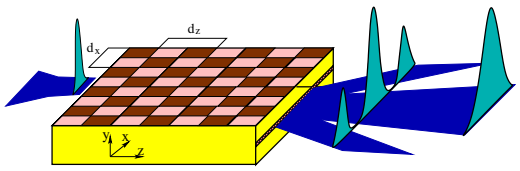


Figure 1: Schematic representation of the periodically modulated optically injected broad area semiconductor amplifier.

The diffractive propagation of a small optical beam along the longitudinal axis of the BAS amplifier can be described by a linear 1+1-dimensional (1D+1D) Schrödinger equation with a periodic potential in both coordinates [12]. By expanding the optical field to a few Bloch modes, this model

can be reduced to a system of ODEs. Its analysis gives a deep understanding of the impact of different parameters (modulation depth and periods, amplifier length, linewidth enhancement factor) to the amplification and the angular shaping of the emitted field.

For simulations of small and moderate beams along periodically modulated BAS amplifiers, the spatio-temporal 2+1-dimensional traveling wave (2D+1D TW) model [9, 14] which describes the spatio-temporal dynamics and nonlinear interactions of the optical fields, induced polarizations and carrier density is applied. Even though the gain saturation reduces the modulation depth at different positions of the BAS device, the obtained results (compression of the emission divergence) are in a good agreement with the linear model analysis.

Precise dynamic simulations of BAS devices and tuning/optimization of the model with respect to one or several parameters require huge CPU time and memory resources. Dynamic simulations of such devices can easily take one or even several days of computations on a single processor computer. Some speed-up of computations can be achieved by using problem-dependent relations of the grid steps, including also variable steps in the lateral dimension. All these grid optimizations, however, are not sufficient when one- or a few- parameter studies should be performed. For this reason, the required computations are performed by means of parallel solvers [15, 16] on parallel compute cluster at the Weierstrass Institute in Berlin.

# 2 MODEL EQUATIONS

## 2.1 Traveling wave model

To simulate a unidirectional beam propagation and amplification in periodically modulated broad area semiconductor amplifier (see Fig. 1), the 2D+1D TW model is applied. According to this model, the spatio-temporal dynamics of the optical field is governed by the following set of equations:

$$\begin{aligned} &\tfrac{n_g}{c_0}\partial_t E = \Big[-\partial_z - \tfrac{i}{2k_0 n_b}\partial_x^2 + \tfrac{g(N,|E|^2)}{2} + i\,\tilde{n}(N) - \big[\tfrac{\alpha}{2} + i\,\delta_0\big] - \mathcal{D}\Big]\,E, \\ &\mathcal{D}E = \tfrac{\overline{g}}{2}\,(E-P)\,, \quad \partial_t P = \overline{\gamma}\,(E-P) + i\overline{\omega}\,P, \\ &E(0,x,t) = \mu(x,t) = \mu_i e^{-x^2\ln(4)/\sigma_i^2}\,e^{i\omega_i t}, \end{aligned} \tag{1}$$

where $E(z,x,t)$ is a slowly varying complex amplitude of the optical field propagating along the longitudinal axis of the BAS amplifier, $|E|^2$ denotes a local photon density, the linear operator $\mathcal{D}$ and the induced polarization function $P(z,x,t)$ model a Lorentzian approximation of the material gain dispersion [17], whereas the complex function $\mu(x,t)$ represents an optically injected Gaussian beam. The gain and the refractive index change functions

$$g = \eta\frac{g'\ln\left(N/N_{\rm tr}\right)}{1+\varepsilon|E|^2}, \qquad \tilde{n} = \eta k_0\sqrt{\sigma N} \tag{2}$$

couple the field equations to the diffusive rate equation for carrier density $N(z,x,t)$,

$$\partial_t N = d_N\partial_x^2 N + \frac{\bar{J}\zeta(z,x)}{qd} - \big(AN + BN^2 + CN^3\big) - \frac{c_0}{n_g}\Re e\big[E^*(g(N,|E|^2) - 2\mathcal{D})E\big], \tag{3}$$

whereas the spatial current modulation function

$$\zeta(z,x) = 1 + \operatorname{sign}\left[\sin\left(2\pi z/d_z\right)\sin\left(2\pi x/d_x\right)\right] \tag{4}$$

represents the spatially periodic electrical contact (see Fig. 1).

In all simulations and analysis the following parameters have been used: the central wavelength $\lambda_0 = 1\,\mu$m, the background refractive index $n_b \in [2.5, 3.725]$, the group velocity index $n_g = 3.6$, the depth of the active zone $d = 15\,$nm, the length of the device $L \in [1.6, 6.4]\,$mm, the width of the device $w = 200\,\mu$m, the differential gain $g' = 25\,\text{cm}^{-1}$, the refractive index change factor $\sigma = 1 \cdot 10^{-25}\,\text{cm}^3$, the transparency carrier density $N_{\text{tr}} = 1 \cdot 10^{24}\,\text{m}^{-3}$, the internal absorption $\alpha = 1.5\,\text{cm}^{-1}$, the static detuning $\delta = 0\,\text{cm}^{-1}$, the nonlinear gain compression $\varepsilon = 5 \cdot 10^{-18}\,\text{cm}^3$, the carrier diffusion coefficient $D_N = 21\,\text{cm}^2/\text{s}$, three carrier recombination parameters $A = 0.3\,\text{ns}^{-1}$, $B = 2 \cdot 10^{-10}\,\text{cm}^3/\text{s}$, $C = 2.5 \cdot 10^{-30}\,\text{cm}^6/\text{s}$, the mean injection current density $\bar{J} = 10\,\text{A/mm}^2$, the lateral period of electrical contact $d_x = 4$ or $8\,\mu$m, the longitudinal period of electrical contact $d_z = 100$ or $400\,\mu$m, the Lorentzian gain amplitude, half width at half maximum, and gain peak detuning $\overline{g} = 100\,\text{cm}^{-1}$, $\overline{\gamma} = 60\,\text{ps}^{-1}$, and $\overline{\omega} = 0\,\text{ps}^{-1}$, the frequency of the optical injection $\omega_i = 0\,\text{ps}^{-1}$, the FWHM of the optical injection intensity $\sigma_i = 20\,\mu$m, and the scaling factor $\eta \in [1, 3]$ for the gain and index change functions $g$ and $\tilde{n}$. For more detailed description of these parameters see Refs. [9, 13, 17].

It will be shown, that the beam quality improvement requires the selection of the spatial periods $d_x$ and $d_z$ satisfying the following relation:

$$\mathcal{Q} = \frac{2d_x^2 n_b}{d_z \lambda_0} = \frac{2k_0 n_b q_z}{q_x^2} \approx 1, \qquad \text{where} \qquad k_0 = \frac{2\pi}{\lambda_0}, \quad q_x = \frac{2\pi}{d_x}, \quad q_z = \frac{2\pi}{d_z}. \tag{5}$$

Once $n_b = 3.125$ and $\lambda_0$, $d_x$, $d_z$ have the values defined above, the resonance condition $\mathcal{Q} = 1$ holds. For simplicity, in the following simulations the value of factor $\mathcal{Q}$ was tuned by modifying the parameter $n_b$.

## 2.2 Reduced models

The 2D+1D TW model can be significantly simplified by neglecting a small impact of the gain dispersion (omit polarization $P$ by setting $\overline{g} = 0$), nonlinear gain compression ($\varepsilon = 0$), adjusting $\omega_i = 0$ and assuming $|E|^2 \ll 1$, which allows an elimination of $N$ from the field equations (1). In this case, the stationary field equations can be efficiently approximated by a 1D+1D linear Schrödinger equation with a periodic potential $\beta(z,x)$ [12]:

$$\begin{aligned} &\partial_z E = \tfrac{-i}{2k_0 n_b}\partial_{xx} E + \beta(z,x)E, \qquad E(0,x) = \mu(x,0), \\ &\beta(z,x) = \bar{\beta} + (1 + i\alpha_H) a_m \sin\left(q_z z\right)\sin\left(q_x x\right). \end{aligned} \tag{6}$$

Here, the complex factor $\bar{\beta}$ gives a fixed spatially uniform contribution (gain and index detuning) to the potential $\beta(z,x)$, whereas $\alpha_H$ and $a_m$ are the linewidth enhancement factor and the harmonic modulation amplitude, both depending on the parameters of the TW model (1–4). When solving Eq. (6), one can assume that $\bar{\beta} = 0$ since the original field function can be recovered afterwards by a simple transformation $E_{orig}(z,x) = E(z,x)e^{\bar{\beta}_{orig} z}$.

Next, by assuming the amplifier width $w \to \infty$, representing the field function $E(z,x)$ in Eq. (6) as the sum of three Bloch modes

$$E(x,z) = e^{-ik_x x}\left(a_0(z) + a_{+1}(z)e^{-iq_x x + iq_z z} + a_{-1}(z)e^{iq_x x + iq_z z}\right),$$

and omitting the resulting fast rotating terms, one arrives to the following system of ODEs:

$$\frac{d}{dz}\vec{a} = \frac{iq_x^2}{2k_0 n_b}\begin{pmatrix} \left(\frac{k_x}{q_x}\right)^2 & c & -c \\ c & \left(\frac{k_x}{q_x}+1\right)^2 - \mathcal{Q} & 0 \\ -c & 0 & \left(\frac{k_x}{q_x}-1\right)^2 - \mathcal{Q} \end{pmatrix}\vec{a}, \qquad c = \frac{k_0 n_b(\alpha_H - i)a_m}{2q_x^2}, \tag{7}$$

where $\vec{u}$ denotes a three-component complex-valued vector, $\vec{u} = (u_0, u_{+1}, u_{-1})^T$. The solution of the linear system of ODEs (7) can be written as

$$\vec{a}(z) = \sum_{l=1}^{3} \vec{A}^{(l)} e^{-ik_z^{(l)} z} \tag{8}$$

where $-ik_z^{(l)}$ and $\vec{A}^{(l)}$ are ($k_x$-dependent) complex eigenvalue and eigenvector of the related spectral problem, such that $\sum_{l=1}^{3} \vec{A}_0^{(l)}(k_x) = \mu(x,0)e^{ik_x x}$.

# 3 Simulations and analysis of the reduced models

## 3.1 Analysis of the reduced ODE model

Fig. 2 shows the dependence of normalized wave vectors $k_z$ on the small radiation angle $\gamma_o \approx k_x/k_0$ for five different values of $\mathcal{Q}$. The imaginary parts of the complex wave-vector components $k_z$ (upper panels of Fig. 2) represent the modal gain so that the FF of the beam radiated from the *long* BAS amplifier at each angle $\gamma_o$ should be mainly determined by the mode with the maximal gain at this $\gamma_o$. Thus, for the factor $\mathcal{Q}$ which is only slightly larger than 1 one can expect an amplification of the optical field radiated around $\gamma_o = 0$ (column (c) of Fig. 2) and, therefore, a significant shaping of the FF at these angles. On the other hand, the FF at the other values of $\mathcal{Q}$ should have a double-peak structure (see maximal gain curves in other panels of Fig. 2).

It is noteworthy that the maximum mode gain value $\Im m(k_z) \approx 4 \cdot 10^{-5}\, k_0$ achieved at $\mathcal{Q} = 1.005$ and $\gamma_o = 0$ (see upper panel of Fig. 2(c)) doubles the emission power at this angle in, approximately, $1.4$ mm long BAS amplifier. Thus, in order to improve the beam shaping in amplifiers of moderate (only a few of mm) length independently on the lateral profile of the initial beam, one should choose the design of the device following the following suggestions. First, the factor $\mathcal{Q}$ should be slightly larger than 1. Second, the modulation amplitude $a_m$ should be as large as possible, what implies the enhancement of the mode gain. Finally, one should properly control the value of the linewidth enhancement factor $\alpha_H$ in order to keep the width of the maximum mode gain around $\gamma_o = 0$ at $\sim 0.5^\circ$.

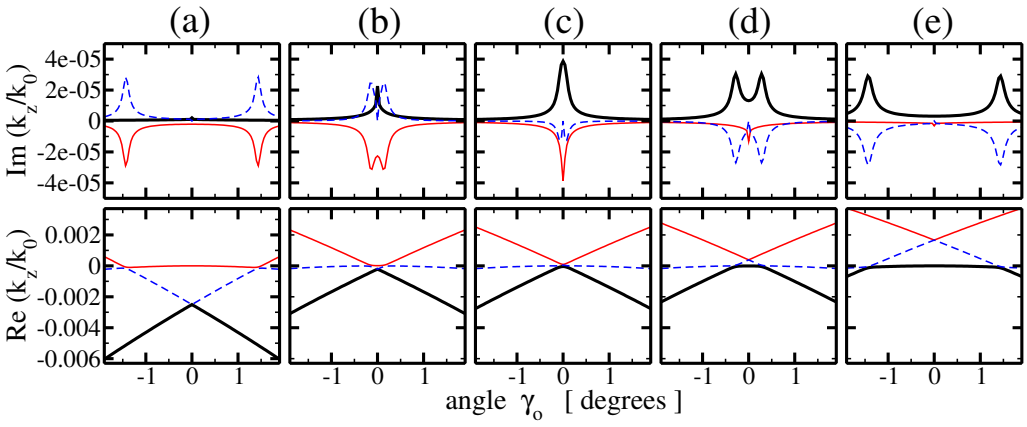


Figure 2: Mode wave-vectors $k_z$ in dependence on radiation angle $\gamma_o$ and $\mathcal{Q}$. First row: mode gain/absorption profiles. Second row: shift of the real wave-vectors. Columns (a), (b), (c), (d), and (e) represent computations with $\mathcal{Q} = 0.8$, $0.98$, $1.005$, $1.04$, and $1.2$, respectively. In all simulations $\eta = 3$, $d_x = 4\,\mu$m, $d_z = 100\,\mu$m, whereas all other parameters are determined in Section 2.

### 3.2 Shaping of the far fields

As it was mentioned above, in the small optical field case the TW model (1–4) can be efficiently replaced by the linear Schrödinger equation (6) and, further, by the system of ODEs (7). In order to justify the analysis of the system (7) discussed in the previous Subsection the simulations of (6) were performed using $\bar{\beta} = 0$, whereas $a_m$ and $\alpha_H$ were defined by the parameters determined in Section 2. The effects predicted above for $\mathcal{Q} \approx 1$ can already be recognized when analyzing the radiated field from the 1.6 mm long BAS amplifier: see the second and the third columns of Fig. 3, where parameters $\eta = 3$, $(d_x, d_z) = (4, 100)\,\mu$m, and $\mathcal{Q} = 0.98$ or $\mathcal{Q} = 1.04$, respectively, were used. In the first column of the same figure, a similar propagation of the injected beam in the non-modulated BAS amplifier is shown.

One can see, that the spatial modulation of $\beta(z, x)$ induces the deformation of the middle lobe of the FF (middle row panels of columns 2 and 3 in Fig. 3). For $\mathcal{Q} = 0.98$ (second column), a dip on the top of the middle lobe of the FF is formed, what corresponds to the double-peak form of the modal gain of the dominant mode (indicated by the blue dashed curve in Fig. 2(b)). A reverse deformation of the FF is seen for $\mathcal{Q} = 1.04$ (third column). Here, the steepening of the FF lobe in the vicinity of $\gamma_o = 0$ is due to the growth of the dominating mode (black solid curve in Fig. 2(d)) at $\gamma_o \approx 0$, and the simultaneous decay of the other mode (blue dashed curve in Fig. 2(d)), which has a dominant primary contribution at $\gamma_o \approx \pm 0.5^\circ$. Thus, in the case of the shorter devices both the initial contributions and the gain profiles of the modes play a role in shaping the propagating beam.

Large angular span far fields are shown in the upper row panels of Fig. 3. One can see, that the shaping of the central FF lobe is supplemented with additional radiation at two opposite angles $\gamma_o \approx \pm\lambda_0/d_x$, corresponding to the relation $k_x \approx \pm q_x$ and resulting from the non-vanishing contributions of the mode amplitudes $a_{\pm 1}$ in Eq. (7). The indirect indication of the side angle

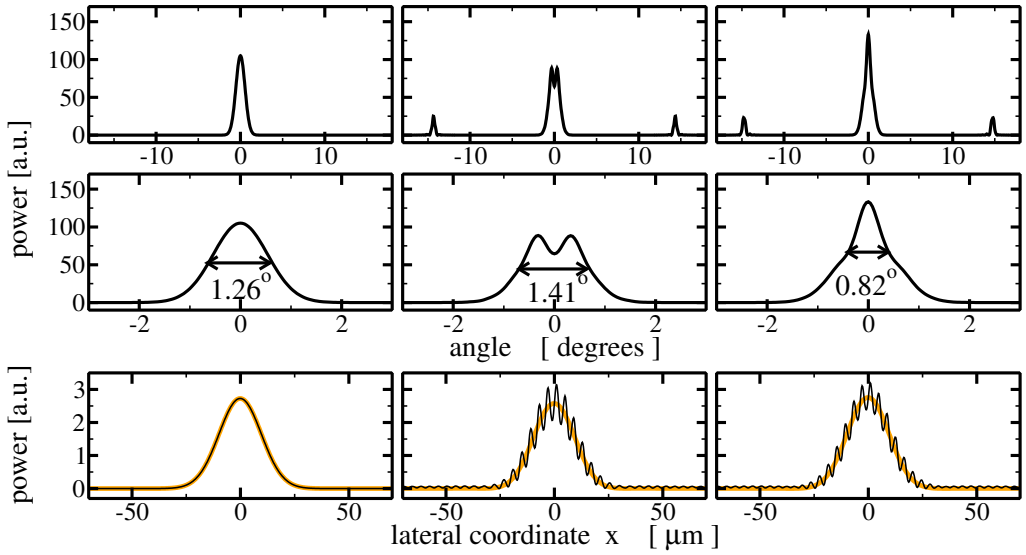


Figure 3: Simulated beam propagation in BAS amplifier according to the model (6) without modulation of $\beta$, i.e., $a_m$ = 0 [first column], with $\mathcal{Q} = 0.98$ [second column], and with $\mathcal{Q} = 1.04$ [third column]. From top to bottom: the large span of the FF [first row], the FF around the central lobe [second row], and the corresponding full (black) and small-scale-averaged (orange) near fields [third row].

radiation is also given by the rapidly oscillating near field intensities (solid black curves in the third row panels). Thick orange curves in these panels represent small-scale averaged near fields [4], which were obtained by omitting large wave-number components of the near fields.

### 3.3 Importance of the factor $\mathcal{Q}$

Several other modulated devices with $d_x$ and $d_z$ such that the factor $\mathcal{Q}$ is far from the resonance condition have been simulated. A comparison of these simulations is given in Fig. 4.

The first two columns of Fig. 4 represent simulations performed on the devices with the parameters satisfying resonance condition $\mathcal{Q} \approx 1$. In the first column of this figure, one can see the behavior of the periodically modulated BAS amplifier already discussed before (only $\eta = 2.5$ in this case). The first and the second row panels show the FF and the FWHM of the central FF lobe for different factors $\mathcal{Q}$. Whereas for $\mathcal{Q} \in [0.9, 1]$ the middle FF lobe becomes broader, for $\mathcal{Q} \in [1, 1.1]$ it is narrowing. The narrowest and highest central FF lobe is observed at $\mathcal{Q} = 1.04$ (see also the right column panels of Fig. 3). Here, some radiation at the side angles can be lost. However, the amplification factor (which is the ratio of the emitted field intensity to the intensity of the emitted field by a similar non-modulated amplifier) of the radiation within the central angle at this $\mathcal{Q}$ is close to one: see the orange curve at the left third row panel of Fig. 4.

It was mentioned before, that the maximum mode gain $\Im m\, k_z(k_x)$ (which is the deciding factor in shaping and amplification of the beam) can be increased by increasing the modulation amplitude $a_m$. Some improvement of the gain and index modulation contrast in BAS devices can

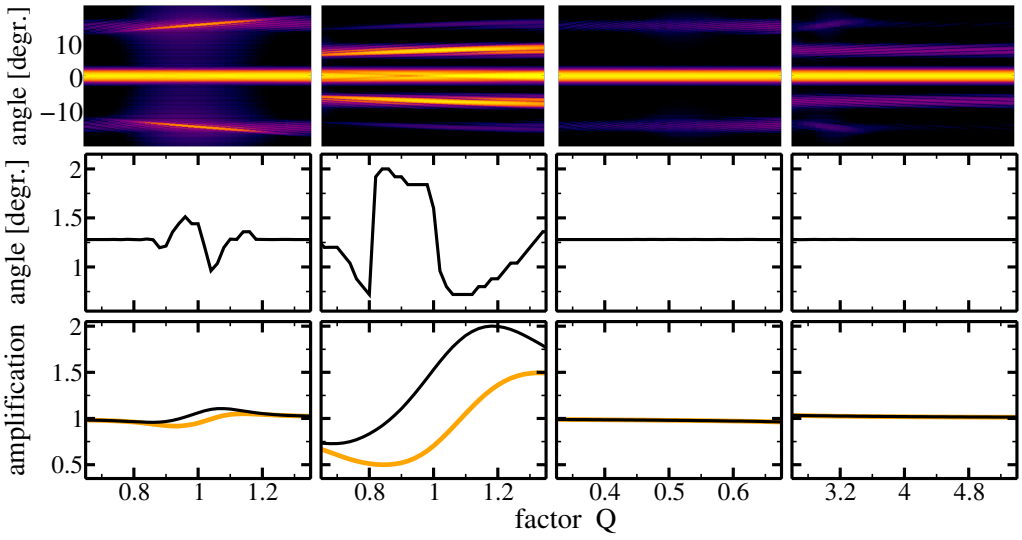


Figure 4: Simulated beam propagation in BAS amplifiers according to Eq. (6) for $\eta = 2.5$ and $(d_x, d_z) = (4, 100)\,\mu$m [first column], $(8, 400)\,\mu$m [second column], $(4, 200)\,\mu$m [third column], $(8, 100)\,\mu$m [fourth column]. All other parameters are like in Fig. 3. First row: mapping of the far fields in logarithmic scale. Second row: the FWHM of the central FF lobe. Third row: the amplification factor of the whole emitted field (black) and its small-scale average (orange).

be achieved by increasing the modulation period $d_x$ (comparing to $d_x = 4\,\mu$m used in all the examples before), and, therefore, decreasing the carrier smoothening by the carrier diffusion. The second column of Fig. 4 shows the behavior of the device with the doubled value of $d_x$ and four-times increased $d_z$, which allows to keep the condition $\mathcal{Q} \approx 1$ satisfied. The modulation amplitude $a_m$ in this case is more than doubled. The field radiation at the side angles is much greater, what is indicated by the significant difference of a full and the small-scale-averaged field intensities in the third row panel. Like in the previous example, the broadening and the narrowing of the middle FF lobe are observed for $\mathcal{Q} < 1$ and $\mathcal{Q} > 1$, respectively. Apparently, the beam shaping at $\mathcal{Q} \in [1.06, 1.1]$ is much more pronounced now. It is also noteworthy, that even though the significant side-band radiation can be lost, the central angle radiation at these $\mathcal{Q}$ is still higher than the power of the field radiated by a similar non-modulated device (orange curve in the third row panel).

The remaining two columns of Fig. 4 represent the devices with the non-resonant relation of the modulation periods, $\mathcal{Q} \approx 0.5$ and $\mathcal{Q} \approx 4$. One can clearly see that even though some small side-angle radiation at $\gamma_o \approx \pm\lambda_0/d_x$ (upper panels) is present, the simulated far and near fields remain insensitive to the changes of $\mathcal{Q}$ that is far away from the resonance $\mathcal{Q} = 1$. It is noteworthy that a similar, insensitive to the variation of $n_b$, behavior can be obtained when simulating a striped contact BAS device [6] with only laterally modulated $\beta$ (only lateral modulation with a period $d_x$ is present), or a standard BAS device without any modulation of $\beta$.

# 4 Simulations of the TW model

Finally, the beam shaping in realistic BAS amplifiers have been analyzed. For this reason, the simulations of the beam propagation and amplification in non-modulated and two different modulated $L = 6.4\,\text{mm}$ long BAS amplifiers using the TW model (1–4), factor $\eta = 1$, and other parameters defined in Section 2 were performed. The results of these simulations for BAS amplifiers are summarized in Fig. 5.

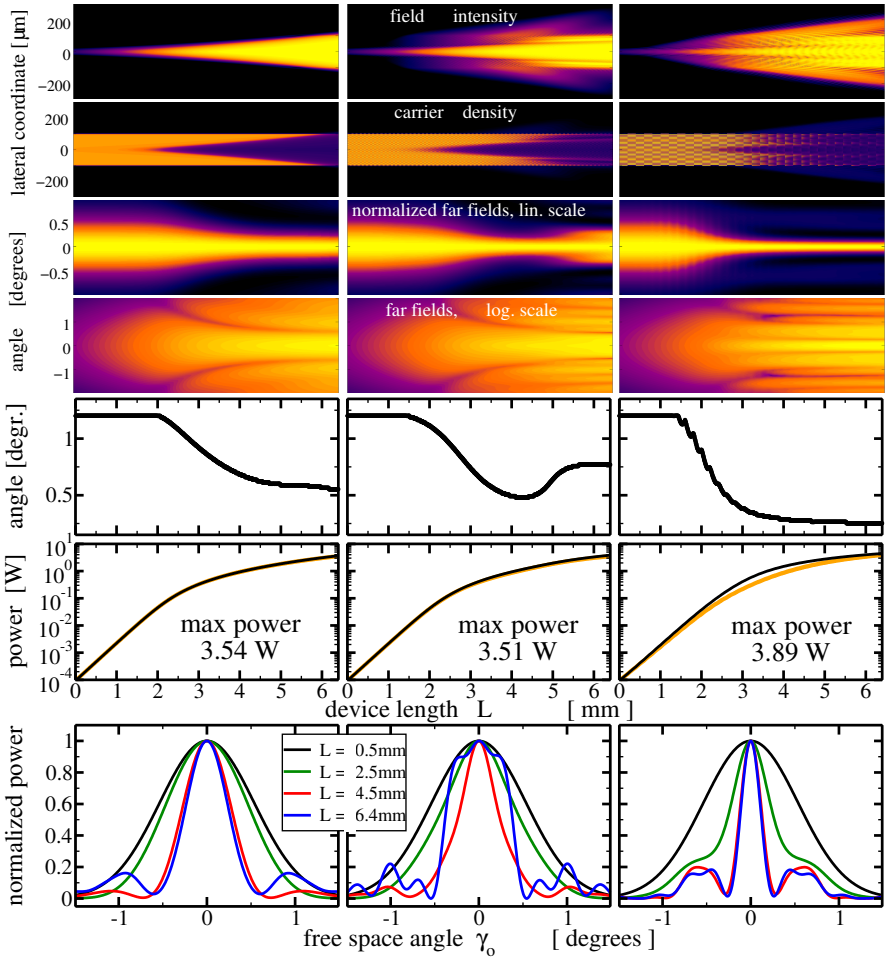


Figure 5: Beam propagation in non-modulated (left), modulated with $(d_x, d_z) = (4, 100)\mu$m (middle), and $(d_x, d_z) = (8, 400)\mu$m (right) BAS amplifiers according to Eqs. (1–4). Injected beam intensity was 0.1 mW, factor $\mathcal{Q} = 1.04$, $\eta = 1$, whereas all other parameters are given in Section 2. 1st-4th rows: mappings of the field intensity, the carrier density distribution, normalized and non-normalized FF recorded and computed for different longitudinal positions (different lengths) of the amplifier. 5th and 6th rows: FWHM of the central FF lobe and the field intensity at corresponding longitudinal position. 7th row: central part of the FF at four different longitudinal positions.

Since the injection of the time independent Gaussian beam is assumed, all lateral field intensity

and carrier density distributions at fixed positions $z$ can be interpreted as field and carrier distributions at the right end of some BAS amplifier of length $L = z$. The intensity of the injected beam is $0.1$ mW. It is sufficiently small, so that the gain compression is nearly absent, and an exponential growth of the field intensity is registered for $z \leq 2.5$ mm (see a linear growth of the curves in 6 row panels of Fig. 5). The comparison of the simulations in this regime with the results of the linear theory derived and discussed above are in perfect qualitative and quantitative agreement. On the other hand, the beam intensity for $z > 4$ mm becomes rather high and saturates the gain (see depletion of carrier densities in the second row panels), what, consequently, leads to the saturation of the field intensity itself. It is noteworthy, that the depletion of the carrier densities at large $z$ can also imply a narrowing of the far fields (see the FF profiles for $L \geq 4.5$ mm in the lower row of the left column of Fig. 5). A further beam narrowing of such type in conventional BAS amplifiers, however, leads to the self-focusing and filamentation, which again degrades the quality of the emitted beam.

The spatial distribution of the carriers, gain and index functions at large $z$ in modulated BAS devices still show well recognizable modulation periods $d_x$ and $d_z$. The local averages and modulation amplitudes (defined by the fixed factors $\bar{\beta}$ and $a_m$ in the linear modeling approach (6)), however, are no more uniform in space. This suggests deviations from the linear theory results discussed in Section 3.

Even though, that the quantitative agreement for larger $z$ is lost, the Fig. 5 still demonstrates a significant beam amplification and shaping in modulated BAS devices (see second column of Fig. 5 for $L \approx 4\mu$m, third column for $L > 3\mu$m, and note the maximal emitted power in the 6th row of the figure). For the devices with the fine modulation period the beam shaping effect is, however, small (compare first and second columns of Fig. 5). For longer devices ($L > 5$ mm) the field emission at the angles $\pm[0.3, 0.8]^\circ$ increases, what reduces the beam quality again. A more optimistic situation is observed for the BAS amplifiers with larger modulation periods (right column of Fig. 5). The FF compression is significantly enhanced, whereas the field emission intensity is also slightly increased.

# 5 CONCLUSIONS

To conclude, it is shown that a spatial modulation of the bias current in BAS amplifiers with a length on the order of a few millimeters can lead to a substantial improvement of the spatial structure of the amplified beam. The study is performed, using a 2D+1D TW model, under realistic semiconductor parameters and technically realizable modulation periods. Beyond what is here presented, this new technique could be implemented to improve the spatial quality of emission of BAS lasers.

# Acknowledgments

The work of M.R. was supported by DFG Research Center MATHEON “Mathematics for key technologies: Modelling, simulation, and optimization of real-world processes”. M.B., R.H. and

K.S acknowledge financial support of Spanish Ministerio de Educación y Ciencia and European FEDER (project FIS2011-29734-C02-01).

# References

[1] T. Burkhard, M.O. Ziegler, I. Fischer, and W. Elsäßer, "Spatio-temporal dynamics of broad area semiconductor lasers and its characterization," *Chaos Solitons Fractals* **10**, pp. 845–850, 1999.

[2] H. Adachihara, O. Hess, E. Abraham, P. Ru, and J. Moloney, "Spatiotemporal chaos in broad-area semiconductor laser," *J. Opt. Soc. Amer. B* **10**(4), pp. 658–665 , 1993.

[3] L. Goldberg and M. Chun, "Injection locking characteristics of a 1 W broad stripe laser diode," *Appl. Phys. Lett.* **53**, p. 1900, 1988.

[4] M. Radziunas and K. Staliunas, "Spatial rocking in broad area semiconductor lasers," *Europhysics Letters* **95**, pp. 14002, 2011.

[5] S. Mandre, I. Fischer, and W. Elsäßer, "Control of the spatiotemporal emission of a broad-area semiconductor laser by spatially filtered feedback," *Opt. Lett.* **28**, p. 1135–1137, 2003.

[6] A. Jechow, M. Lichtner, R. Menzel, M. Radziunas, D. Skoczowsky, and A. Vladimirov, "Stripe-array diode-laser in an off-axis external cavity: Theory and experiment," *Optics Express* **17**(22), pp. 19599–19604, 2009.

[7] M. Lichtner, V.Z. Tronciu, and A.G. Vladimirov, "Theoretical investigation of striped and non-striped broad area lasers with off-axis feedback," *IEEE J. of Quantum Electron.* **48**(3), pp. 353–360, 2012.

[8] B. Sumpf, K.-H. Hasler, P. Adamiec, F. Bugge, F. Dittmar, J. Fricke, H. Wenzel, M. Zorn, G. Erbert, and G. Tränkle, "High-brightness quantum well tapered lasers," *IEEE J. Select. Topics in Quantum Electron.* **15**, pp. 1009–1020, 2009.

[9] M. Spreemann, M. Lichtner, M. Radziunas, U. Bandelow, and H. Wenzel, "Measurement and simulation of distributed-feedback tapered master-oscillators power-amplifiers," *IEEE J. of Quantum Electron.* **45**(6), pp. 609–616, 2009.

[10] K. Staliunas, R. Herrero, and R. Vilaseca, "Subdiffraction and spatial filtering due to periodic spatial modulation of the gain-loss profile," *Physical Review A* **80**, p. 013821, 2009.

[11] M. Botey, R. Herrero, and K. Staliunas, "Light in materials with periodic gain-loss modulation on a wavelength scale," *Physical Review A* **82**, p. 013828, 2010.

[12] R. Herrero, M. Botey, M. Radziunas, and K. Staliunas, "Beam shaping in spatially modulated broad area semiconductor amplifiers," *Optics Letters* **37**(24), pp. 5253–5255, 2012.

[13] M. Radziunas, M. Botey, R. Herrero, and K. Staliunas, "Intrinsic beam shaping mechanism in spatially modulated broad area semiconductor amplifiers," *Appl. Phys. Lett.* **103**(13), p. 132101, 2013.

[14] S. Balsamo, F. Sartori, and I. Montrosset, "Dynamic beam propagation method for flared semiconductor power amplifiers," *IEEE J. Select. Topics in Quantum Electron.* **2**, pp. 378–384, 1996.

[15] I. Laukaitytė, R. Čiegis, M. Lichtner, and M. Radziunas, "Parallel numerical algorithm for the traveling wave model," in *Parallel Linear Algebra and Optimization: Advances and Applications*, R. Čiegis, D. Henty, B. Kågström and J. Žilinskas, eds., *Springer Optimization and Its Applications* **27**, pp. 237–250, Springer, 2009.

[16] R. Čiegis, M. Radziunas, and M. Lichtner, "Numerical algorithms for simulation of multisection lasers by using traveling wave model," *Math. Model. Anal.* **13**(3), pp. 327–348, 2008.

[17] U. Bandelow, M. Radziunas, J. Sieber, and M. Wolfrum, "Impact of gain dispersion on the spatio-temporal dynamics of multisection lasers," *IEEE J. of Quantum Electron.* **37**, pp. 183–188, 2001.